Smart Underground Antenna Arrays: A Soil Moisture Adaptive Beamforming Approach

Abdul Salam and Mehmet C. Vuran

Cyber-Physical Networking Laboratory
Department of Computer Science & Engineering
University of Nebraska-Lincoln, Lincoln, NE 68588
Email: {asalam, mcvuran}@cse.unl.edu

***Abstract*—In this paper, a novel framework for underground beamforming using adaptive antenna arrays is presented. Based on the analysis of propagation in wireless underground channel, a theoretical model is developed which uses soil moisture information and feedback mechanism to improve performance wireless underground communications. Array element in soil has been analyzed empirically and impacts of soil type and soil moisture on return loss and resonant frequency are investigated. Beam patterns are investigated to communicate with both underground and above ground devices. Depending on the incident angle, refraction from soil-air interface has the adverse effects in the UG communications. It is shown that beam steering improves the UG2UG communications by providing the high gain lateral wave. It is also shown that angle which enhances lateral wave is a function dielectric properties of the soil which is affected by moist and texture of soil and it varies from 0° to 16° with soil moisture variations. It is shown that for low soil moisture content optimal UG lateral angle is high and it decreases with change in soil moisture. Planar array structures are considered and different optimization approach has been developed to improve the performance of soil moisture adaptive beamforming.**

I. Introduction

Soil properties and soil moisture significantly impact the underground (UG) communications [1]. This necessitates the adaption of parameters of the UG communication system based on the changing environment. Such adaption requires tight integration of soil sensing technologies with the communication devices to enable optimum performance of UG communication system. For UG antenna, change in soil moisture requires changing operation frequency and bandwidth to maintain high throughput and gain [2]. Similarly, to enhance the lateral wave in the UG communications, maximum energy should be focused at a particular angle which should be determined dynamically by the soil properties in the areas surrounding the buried UG antenna [1]. Due to these phenomenons, the use of high gain directional antennas [3], [4], lacking the capability to adjust its beam direction according to the environment may not result in ideal system performance. Therefore, a soil SMABF approach based on antenna arrays is required which could adjust its parameters and could beam the maximum energy at the desired angle.

In [1], propagation characteristics of wireless UG communications has been modeled and lateral wave has been shown to be most dominant component of the UG communications [5], [6], [7]. The lateral component has the potential, due to its lower attenuation, to reach higher distances. This lateral wave is formed and carries the most energy when antenna orientation is at a specific angle. This angle varies with variations in soil moisture and also depends on soil properties such as soil texture, and bulk density. On the contrary, for UG2AG communication, energy from UG antenna needs to be directed vertically in order to avoid refraction losses at the soil-air interface.

Many factors impact the beamforming from UG antenna arrays. The distance that waves travel from the antenna element to reach at soil air interface is different for each array elements based on the array geometry. Change in index of refraction causes delay in the speed of beams. Soil moisture variations lead to change in the resonant frequency of antenna elements. Bandwidth, return loss, and reflection coefficients at the resonant frequency also change with soil moisture. UG2UG and UG2AG communications require different beam shapes from UG antenna array. In UG2UG communications, lateral wave is the most dominant and travels along the soil-air interface. In UG2AG energy needs to be focused in the broadside. Differences in wave propagation in these two links require different angles at which waves should be incident at soil-air interface. Due to these factors, adjustment of the phase at the UG antenna elements need phase alignment to add up coherently to avoid errors in beam steering and beam pointing direction. SMABF is used to align signal envelops and archives the desired performance across the frequency spectrum.

Moreover, a reliable beamforming architecture requires deep understanding of the propagation in the wireless communication channel to exploit nature of spatial properties of multipath components for an effective beamforming solution. Despite the recent developments in wireless UG communications, the communication ranges are still limited for many potential applications. Therefore, advanced techniques, which are designed based on the unique characteristics of the wireless UG channel, are required to extend the communication range. Optimum performance of an UG beamforming antenna depends on the accurate physical insight into the propagation characteristics of the wireless UG channel.

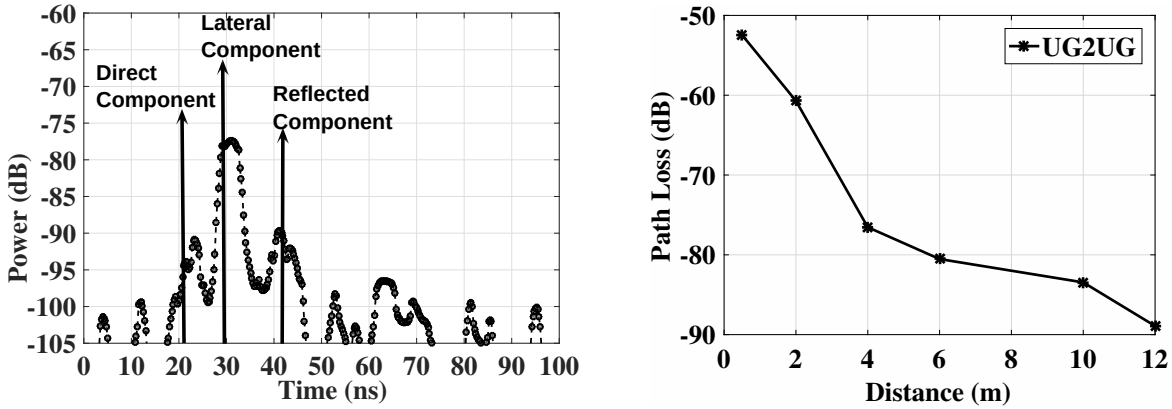

(a) (b)

Fig. 1: (a) A power delay profile (PDP) of the impulse response model of the wireless UG channel [1], (b) Pathloss in UG2UG channel.

II. Organization and Contributions of This Work

This is the first work to propose soil moisture adaptive beamforming (SMABF) for the UG communications. Antenna array structures buried underground are considered which communicate through the soil by using UG channel medium. Based on the receiver position, EM waves either travel completely through soil for UG communications or some part of it goes through the air for aboveground(AG) communications. We analyze the UG channel impulse response model for UG beamforming perspective and identify the major EM wave components. Challenges in UG beamforming are highlighted and use of soil adaptive beamforming approach is motivated. We present the effects of different soil properties on single antenna array element and a soil moisture based optimum steering method is developed for beamforming. This proposed mechanism estimates the best beam steering angle based on the soil moisture sensing. Next, based on the optimal angle, a beam steering method is developed for beamforming. This method works on array element weighting based on the UG2UG and UG2AG communications. Array element positions, inter-element distance are analyzed for best performance. Then an optimization algorithm is developed which is based on the feedback and soil moisture sensing information. Sidelobe reduction is done by using element thinning, and element positions optimization. Performance analysis and results of SMABF communications are presented.

The rest of the paper is organized as follows: the related work is discussed in Section III. The channel model is discussed in Section IV. Challenges to UG beamforming are presented in Section V. Ann antenna array element in soil is analyzed in Section VI. Design of SMABF array and steering algorithm is given in Section VII. Results and optimization techniques are presented in Section VIII. In Section IX, simulation results are shown. Implementation issues are discussed in Section X. We conclude in Section XI.

III. Related Work

SMABF approach has potential applications in many practical scenarios such as precision agriculture, ground penetrating radars (GPR), hazardous object search, locating IEDs, transmission structures under the runways for aircraft communications, antennas for geographic research, communications from marshes, geology, and wireless underground sensor networks (WUSNs). Wireless UG channel is the medium of communication in WUSN. WUSNs are being used in the area of precision agriculture [8], [9], [4], [5], [10], [11], [12], border monitoring [6], [13]. land slide monitoring, and pipeline monitoring [14], [12], [10]. WUSNs are based on both EM based propagation [15] and magnetic induction based communication [16].

Beamforming antennas [17] are being used in wireless networks to reduce interference and improve capacity. Beamforming have been addressed in [18], [19], [20], [21], [22], [23], [24], [25], [26] for over-the-air (OTA) wireless channels and in [27] for MI power transfer, but no existing work has considered the UG beamforming. In UG communications, lateral component [28] has the potential, via beam-forming techniques, to reach at farther UG distances which otherwise are limited ($8\,\mathrm{m}$ to $12\,\mathrm{m}$) because of higher attenuation in soil [1]. Since the UG communication devices are buried at close proximity of soil-air interface in homogeneous soil [8], therefore, soil moisture changes are not abrupt. Analysis of the layered soil effects is left for future investigation. To the best of the author's knowledge, this is the first work to develop soil moisture adaptive UG beamforming for the wireless UG channel.

IV. Channel Model for SMABF

Estimation of propagation characteristics through the soil is crucial to design a UG communication systems. A channel model for UG communications have been developed in [1] and has been validated empirically. Direct, lateral and reflected components have been identified at the UG receiver. A power delay profile (PDP) of wireless UG channel has been shown in Fig. 1(a). Lateral wave is the strongest component as it suffers low attenuation when passes through the air along the soil-air interface as compared to the reflected and direct wave which undergoes higher attenuation due to the high losses in soil medium.

Due to these factors, an impedance-matched antenna for OTA communication is not matched in soil and new designs are necessary. Moreover, due to their buried deployment and the dominance of the lateral wave in the wireless UG channel, sending signals in an isotropic direction (i.e., partly towards the Earth) would be waste of the resources. Thus, in addition to individual antenna design, SMABF aims to communicate with UG and AG devices by forming a focused narrow width beam in the desired direction, hence, extending the communication range.

The UG channel process can be expressed as a sum of direct, reflected and lateral waves and is given as [1]:

$$h_{ug}(t) = \sum_{l=0}^{L-1} \alpha_l \delta(t-\tau_l) + \sum_{d=0}^{D-1} \alpha_d \delta(t-\tau_d) + \sum_{r=0}^{R-1} \alpha_r \delta(t-\tau_r) \ , \tag{1}$$

where L, D, and R are number of multipaths; α_l, α_d, and α_r are complex gains; and τ_l, τ_d, and τ_r are delays associated with lateral wave, direct wave, and reflected wave, respectively.

Unique Features of UG Channel: It is worth noting that the unique interactions between soil, antennas, and the channel create unique opportunities that are not possible in other media. Moreover, due to higher permittivity of soil compared to air, wavelength at a particular frequency is lower than that in air. This allows the use of lower frequency waves, which attenuate less in soil, with smaller-size antennas. This unique phenomenon also allows the design of buried antenna arrays with reasonable sizes. Furthermore, because of unique three-wave structure of the PDP (Fig.1(a)), by focusing the transmitted energy to lateral waves, the delay spread can further be decreased, leading to higher data rates and long-range communications.

Limitations of the UG Channel: Two types of limitations are observed in the UG channel when compared to the OTA wireless channel. These are: i) Communication Range Limitation. High attenuation in the UG channel is one of the limiting factor for long range communications in the UG2UG channel. In Fig. 1(b), attenuation with distance is shown. $30\,\mathrm{dB}$ path loss is observed when UG distance increases from $2\,\mathrm{m}$ to $12\,\mathrm{m}$. ii) Data Rate Limitation. It has been shown in [2], that data rates in the UG channel are limited to few kbps when commodity motes are used for UG communications.

In this work, we exploit the unique features of the UG communication channel to design a novel SMABF architecture which overcome these limitations.

V. Challenges in Underground Beamforming

In this section, we first analyze a fixed-beam system and review UG beamforming challenges. Impact of change of soil moisture on wavelength and directivity are discussed.

Impact of Soil Moisture on Wavelength: Wavelength in soil is calculated as:

$$\lambda_s = \frac{2\pi}{k_s} \tag{2}$$

where k_s is the wave number in soil (Appendix B). In Fig. 2(a), change in wavelength is shown as a function of volumetric water content (VWC). It can be observed that when VWC increases from 20% to 40%, wavelength at $300\,\mathrm{MHz}$ decreases from $21\,\mathrm{cm}$ to $17\,\mathrm{cm}$. Similarly at $400\,\mathrm{MHz}$ wavelength decreases from $17\,\mathrm{cm}$ to $14\,\mathrm{cm}$. Accordingly, the distance between succeeding elements needs to selected in a way to accommodate wavelength changes due to soil moisture variations without affecting the directivity and beam patterns.

Impact of Soil Moisture on Directivity: In Fig. 2(b), directivity pattern is shown with change in soil moisture for antenna elements that are half wavelength $\lambda_0/2$ (in the air) apart. Change in directivity of a 4-element antenna array is shown in Fig. 2(c) for a 15-week soil moisture data collected in a soy bean field during summer crop season in 2015. Directivity is found by using [29]:

$$D \approx 2\frac{Nd}{\lambda_s} \tag{3}$$

where N is the number of elements, d is the distance between elements, and λ_s is the wavelength in soil . It can be observed that soil moisture leads to dynamic changes in directivity, which needs to be mitigated for SMABF.

Phased arrays are used to steer the main beam of the antenna without physically moving the antenna [30], [31], [32]. Due to the requirement of accurate phase control with wavelength change, the smart antennas with phase shifters are suitable in UG communications. However, designing wideband antenna arrays may lead to space and hardware complexity limitations underground. Moreover, the lack of closed-form models for UG antennas make theoretical understanding of UG beamforming challenging. In this work, we study the effects of soil on UG beamforming and design a UG SMABF solution which is robust and adaptive to these variations. To maximize the communication range, signal footprint should be tailored by limiting energy radiation in direct and reflected components as these are attenuated most. SMABF in UG channels is adaptive based on effects of frequency and soil moisture, soil type, depth and distance of system deployment on the UG channel.

VI. Analysis of Single Array Element in Soil

We first analyze the behavior of single antenna array element in soil medium. In this section, first, an antenna element in soil is compared with over-the-air (OTA) antenna element through empirical evaluation by using the testbed shown in Fig. 3. The indoor testbed holds antennas at different depths and distances. The element impedance and soil-air interface effects are analyzed.

Comparison of In-Soil and OTA Array Element: We compare the performance of single array element (dipole) buried in soil to a free space element. In Fig. 2(d), reflection coefficient measurements of a $433\,\mathrm{MHz}$ over-the-air antenna element in three different soils are shown for frequency ranges of $100\,\mathrm{MHz}$ to $500\,\mathrm{MHz}$. It can be observed that the resonant frequencies of the antennas shift to lower frequency values when they are buried underground, due to shorter wavelength in soil. Resonant frequency in silt loam soil is $202\,\mathrm{MHz}$, in

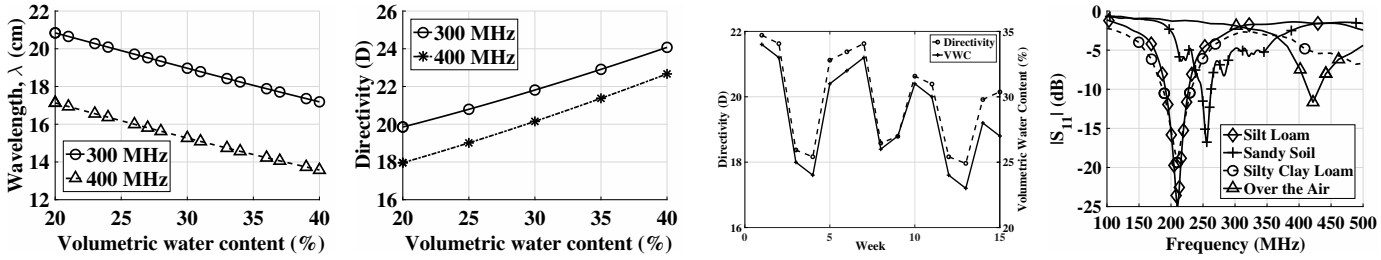

(a) (b) (c) (d)

Fig. 2: (a) Change in wavelength with change in soil moisture (b) Array directivity with change in soil moisture, (c) Directivity of antenna in a typical growing season in a soybean field, (d) Reflection coefficients of a dipole element.

silty clay loam it is 209 MHz, and in sandy soil resonant frequency is 278 MHz. Resonant frequency in sandy soil is 76 MHz higher than the silt loam soil. This is because the relative permittivity of a particular soil depends on its net water content [33] and silt loam has a higher water holding capacity than sandy soil. Therefore, silt loam has a higher relative permittivity and results in a lower resonant frequency for a given antenna. Next, we analyze the effects of soil moisture variations on the return loss, and resonant frequency of the array element.

Impact of Soil Moisture on Element S_{11}: In Figs. 4, return loss of antenna with change in soil moisture at different depths in sandy soil is shown. In Fig. 4(a), return loss in silt loam at 10 cm depth is shown for soil matric potential values of 0 and 255 CB. When soil moisture decreases (matric potential changes from 0 to 255 CB), resonant frequency has increased from 278 MHz to 305 MHz.

Effects of change in soil moisture on the resonant frequency at different depths are shown in Fig. 4(b). At 20 cm, with change in soil moisture from 0 to 255 CB, resonant frequency has increased from 276 MHz to 301 MHz. With the similar change at 30 cm depth, resonant frequency changes from 276 MHz to 301 MHz and at 40 cm depth, it changes 251 MHz to 279 MHz.

Analysis of the return loss of antenna Fig. 4(a)-4(d)) in sandy soil at different burial depths and soil moisture levels shows that the return loss of the antenna changes with the soil moisture. Resonant frequency moves to lower frequency ranges when the soil moisture increases. Moreover, unlike over-the-air communications, the optimal frequency where the maximum capacity is achieved is not the same as the resonant frequency of the antenna [2].

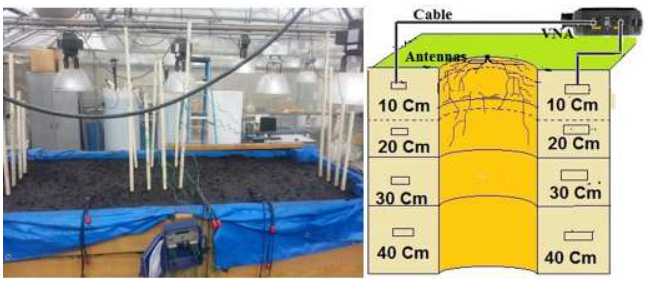

Fig. 3: Layout of the indoor Testbed.

Element Impedance in Soil: A knowledge of impedance of SMABF element in soil is important to match the array to transmission line. For efficient wireless communication, the impedance of an antenna element, Z_a, needs to be matched to the output impedance of the transceiver, Z_s, such that the radiated power is maximized and the returned power to the transmitter is minimized. Due to soil-air interface effects, soil cannot be considered as an infinite medium, as is typically considered in OTA antenna models. Consequently, antenna return loss (RL) is not merely a shift in spectrum space when the antenna is moved from air to soil, but the shape of the RL curve also changes.

Soil-Air Interface Impacts: When a buried antenna is excited, a current distribution of $I_0(\zeta)$ is generated along the antenna. The generated wave propagates towards the soil-air interface, where it is reflected and refracted. The reflected electric field, E_r, that reaches the antenna induces an additional current, I_r, on the antenna, affecting its impedance [34]. The induced current further impacts the generated wave and higher order reflection effects exist. However, due to the high attenuation in soil, these higher order effects are negligible and only the first order effects are considered. The induced current on the dipole, I_r, as well as the resulting impedance, Z_r, can be modeled as the result of a field generated by an imaginary dipole placed in a homogeneous soil environment. Accordingly, Z_r is modeled based on a modified mutual impedance model between two dipole antennas [35] and the reflection coefficient at the soil-air interface. The mutual impedance, Z_r, is then added to the self impedance, Z_a, to obtain the total impedance of the buried antenna in half space [34].

With insights gained from the analysis of individual antenna antenna, we design multi-element SMABF array in the next section.

VII. Design of SMABF Array

In this section, we investigate array configuration and element positioning of phased array antenna for UG communications (Section VII-A). In Section VII-B, beam patterns for UG2AG communications are developed. UG2UG beam patterns are analyzed an in Section VII-C. In these discussions, we directly focus our attention to the beamforming aspects related to the UG2UG and UG2AG communication without going into details of beamforming basics. For comprehensive treatment of the subject, we refer the reader to [36].

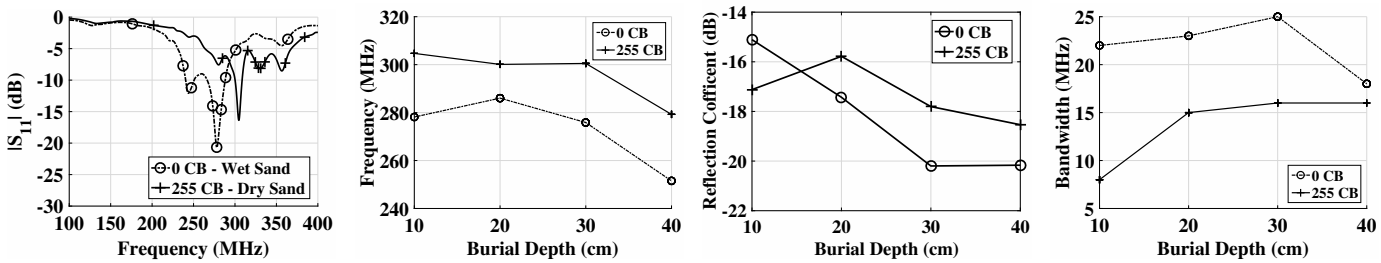

(a) (b) (c) (d)

Fig. 4: Return loss in sandy soil, : (a) S_{11} at different frequencies, (b) Change in resonant frequency with burial depth, (c) Reflection Coefficient (dB) at different burial depths, (d) Antenna bandwidth at different burial depths.

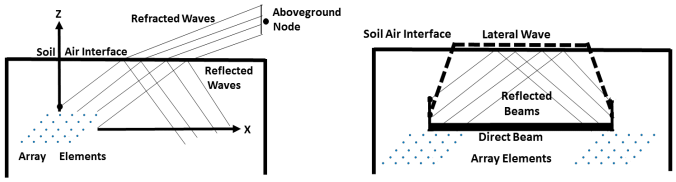

(a) (b)

Fig. 5: Communications schematic for (a) UG2AG communications (b) UG2UG communications.

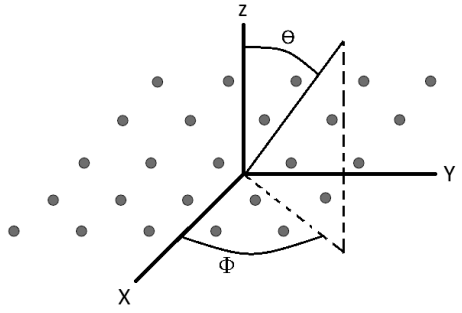

(a)

Fig. 6: Arrangement of array elements into a planar grid.

A. Array Layout and Element Positioning

First, we investigate the optimal size and number of antenna elements in the UG array which can form desired beams to communicate with both UG and AG devices. Second, we analyze UG antenna element spacing.

Following features are desirable while designing an SMABF antenna array: 1) Due to wavelength changes in soil, antenna spacing should be such that the directivity and desired beam shape are not lost significantly with the changes in soil conditions, 2) Array is to be designed to work on wide range of frequencies, 3) Elements are half-wave length with support for multiple inter-element spacing, 4) The array is to have number of elements which are not prohibitive for UG deployment and maintains higher directivity. Higher directivity is achieved by having larger number of elements, 5) Both UG2UG and UG2AG array patterns are desirable with support of steering angles, 6) It should be able to adjust its parameters when the soil moisture changes.

Multi-dimensional arrays structure such as rectangular, planar, and circular arrangements facilitates simultaneous beams in multiple planes [30]. Due to requirement of different array patterns, planar array structure is considered for SMABF approach. Array lies in $x-y$ plane with z direction pointing to the soil-air interface. For AG nodes, the elevation angle θ is measured from normal to soil-air interface. The azimuthal angle ϕ is used to measure steer beams to UG nodes. Beam steering angles for both type of communication links are given in Table I. Dipole elements in the planar array are arranged into a rectangular structure as shown in the Fig. 6(a).

TABLE I: UG2UG and UG2AG Steering Angles.

Communication Link	θ	ϕ
UG2AG - No Steering	$0°$	$0°$
UG2AG - Beam Steering	$0° - 60°$	$0°$
UG2UG - Lateral Wave	VWC Dependant See Section VII-C	$0°$
UG2UG - Direct Wave - X Orientation	$90°$	$0°$
UG2UG - Direct Wave - Y Orientation	$90°$	$90°$

In planar array structure, antenna elements are arranged multidimensional structures to yield the desired radiation pattern suitable for communication with AG devices. Antenna elements are grouped into multiple arrays with different source strength in such a way that source strengths are adjusted to strengthen the lateral wave based on the depth and wave attenuation experienced in the vertical direction [37], [28] (other types of antenna elements are outside of the scope of this paper).

Underground Communication Links: UG nodes communicate with other UG nodes (UG2UG link) and AG nodes (UG2AG link). Communications schematic for UG2AG communications, and UG2UG communications is shown in Figs. 5. These AG nodes can be fixed sinks or mobile nodes mounted on movable infrastructures. In AG communications, waves propagating to receiver nodes are refracted from soil-air interface, whereas in UG communications, lateral waves need to be utilized. Desired beam patterns for both scenarios are shown in Figs. 5. In Fig. 5(a), that refractions and reflections of EM waves from the soil-air interface effect the beam patterns propagating to the AG node.

B. UG2AG Communication Beam Pattern

Since UG to AG communications link is different from UG to UG communication, therefore energy radiated in the vertical direction from the buried UG antenna needs to be determined at different receiver angles. To ascertain the best angle for communication from an UG antenna to AG node, experiments are conducted for UG to AG communication at different receiver angles of the AG node [1].

The UG sender antenna is buried at a depth of $20\,\mathrm{cm}$ and the position of the AG node, mounted on a adjustable height pole, is changed at the soil surface at distances of $2\,\mathrm{m}$, $4\,\mathrm{m}$, $5.5\,\mathrm{m}$, and $7\,\mathrm{m}$ at angles of $0°$, $30°$, $45°$, $60°$, and $90°$.

Measurements are conducted at angles of $0°$, $30°$, $45°$, $60°$, and $90°$ from the sender. It is observed that the for receiver at the angle of $0°$ highest attenuation occurs whereas the lowest attenuation is observed at $90°$. Low attenuation at the $90°$ is caused because of no refraction from soil-air interface. Since at $90°$, the wave does not experience the high refractions in comparison to the $0°$, therefore, for UG2AG communications the energy directed straight up to the soil-air interface leads to higher gains and throughput. In the following, we discuss three scenarios of UG2AG communications.

Case 1: No Steering. Accordingly the array factor for UG2AG pattern can be expressed as [32]:

$$AF(\theta,\phi) = \sum_{i=1}^{N} w_i exp(-\big[jk_s r_i(x_i \sin\theta\cos\phi + y_i \sin\theta\sin\phi)\big]), \tag{4}$$

where N is the number of elements, w_i is the weight of each antenna element, x_i and y_i are i^{th} element coordinates, and wave number in the (Appendix B).

Case 2: Beam Steering. This no-steering pattern is used for forming the broadside beam without taking into account the location of AG nodes. However, if the precise location of the AG node (θ_{AG}, ϕ_{AG}) is known, then beam is steered accordingly by adding the phase shifts δ_i at the i^{th} element to steer a beam to (θ_{AG}, ϕ_{AG}):

$$AF(\theta,\phi) = \sum_{i=1}^{N} w_i exp(-\big[jk_s r_i(x_i \sin\theta\cos\phi + y_i \sin\theta\sin\phi)\big] + \delta_i),$$

where δ_i is given as:

$$\delta_i = -k_s(x_i \sin\theta_{AG}\cos\phi_{AG} + y_i \sin\theta_{AG}\sin\phi_{AG})$$

Case 3: Refraction Adjustment. When UG2AG beam is steered at angles other than normal to the soil-air interface, refraction phenomenas should be taken into account. These effects arise because of the coupling of the wave with soil-air interface. Soil-air interface separates the soil medium form air and both have different properties which give rise to refraction of waves. The index of refraction and refraction process not only degrade the performance of the UG beamforming but also change the angle-of-arrival at the AG nodes. Moreover, an optimal angle of incidence exists with respect to burial depth of the UG antenna array, at which refraction is more dominant and less reflection of incidence wave occurs. Moreover, these phenomena result in different propagation speeds because of different refraction index of soil and air, leading to spreading, and decay of focused beam. Due to these factors, adjustment of the phase at the UG antenna elements does not align the phase to add up coherently and leads to errors in beam steering and beam pointing direction. Depending on the incident angle, this has the adverse effects in the UG communications. The error caused by refraction from soil-air interface is called beam squint [32] and results in time dispersion of the signal.

To address this issue, SMABF uses time-delay beam steering [32] to align signal envelops and achieve the desired performance to mitigate soil-air interface effects. Time delay units are used to adjust the beam pointing direction by using the refraction angle. Given the position of the AG node, (θ_{AG}, ϕ_{AG}), time delay to correct this effect is expressed as:

$$\tau_{\mathsf{mn}} = \begin{pmatrix} \tau_{11} & \tau_{12} & \cdots & \tau_{1n} \\ \tau_{21} & \tau_{22} & \cdots & \tau_{2n} \\ \vdots & \vdots & \ddots & \vdots \\ \tau_{m1} & \tau_{m2} & \cdots & \tau_{mn} \end{pmatrix} \tag{5}$$

where τ_{ij} is calculated as

$$\tau_{ij} = \sin\theta_r[i \times d_i \cos\phi_r + j \times d_j \sin\phi_r]/S, \tag{6}$$

where S is the speed of the wave in soil as given in Appendix C, d_i and d_j are the element spacing in the x and y direction respectively, and θ_r is calculated by using the Snell's law as:

$$\theta_r = \arcsin\left(\frac{\eta_s}{\eta_a}\sin\theta_{AG}\right), \tag{7}$$

where η_a is the refractive index of air, and η_s is refractive index of soil.

In (6), τ_{ij} is a function of burial depth from soil-air interface, and soil moisture. Higher refraction index (slow speed of wave in soil) leads to higher delay.

Once τ_{ij} and δ_i is determined, the array factor is expressed as:

$$AF(\theta,\phi) = \sum_{i=1}^{N} w_i exp(-\big[jk_s r_i(x_i \sin\theta\cos\phi + y_i \sin\theta\sin\phi) + 2\pi f \sum_{j-1}^{M} \tau_{ij} + \delta_i\big], \tag{8}$$

In Section VII-C, we analyze the UG2UG communications beam patterns.

C. UG2UG Communication Beam Pattern

In this section, two scenarios for UG2UG communications are discussed. First, we investigate the optimal angle for soil moisture-based beam steering.

Case - 1: Estimation of Soil Moisture-Based Optimum Steering Angle to Maximize Lateral Wave: It has been shown in [38], [1], that in UG communications lateral wave travels along the soil-air interface to reach the receiver. This

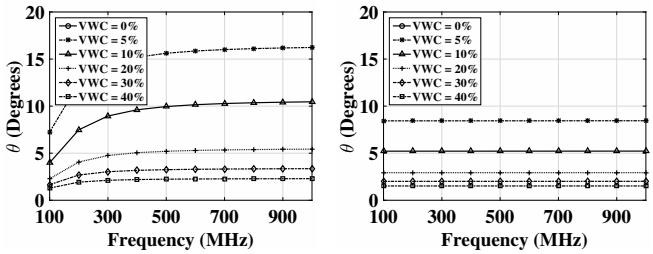

Fig. 7: Optimal angle with frequency in different soils: (a) Silty Clay Loam, (b) Sandy Soil.

lateral wave is maximized if the energy from the UG antenna is radiated in a particular angle. This angle depends on the dielectric properties of the soil and is given as [39]:

$$\theta_{UG} = \frac{1}{2}\tan^{-1}\left(\frac{2Re(n^2-1)^{1/2}}{|n^2-1|-1}\right)rad, \tag{9}$$

where n is the refractive index of the soil and is given as

$$n = \sqrt{\frac{\sqrt{\epsilon'^2+\epsilon''^2}+\epsilon'}{2}}\ , \tag{10}$$

and ϵ' and ϵ'' are the real and imaginary parts of the relative permittivity of the soil. Details of this optimal angle are given in Appendix A.

Case - 2: Direct Wave. For short UG2UG communication distances, when direct wave is more dominant wave than the lateral wave. In this case, communication is enhanced by forming a direct UG beam towards the receiver UG node through the soil. Steering angles for lateral and direct wave beams are given in Table. I. In both cases, (5) is used based on the desired beam pattern.

D. Directivity

Directivity of a SMABF array is defined as:

$$D = \frac{4\pi|AF_{max}|^2}{\int_0^{2\pi}\int_0^{\pi}|AF|^2\sin\theta d\theta d\phi}, \tag{11}$$

where AF_{max} is the main beam peak (maximum of the array factor) is given as:

$$AF_{max} = \sum_{i=1}^{N} w_i, \tag{12}$$

E. SMABF Steering Algorithm

A beam steering algorithm is given in Algorithm 1 to produce different beam patterns required for UG2UG and UG2AG communications. This algorithm addresses the communication requirement on these two separate links.

VIII. Results and Optimization

In this section, first, results of the SMABF are presented and then adaptive SMABF approach is compared with nonadaptive approach. Optimization techniques are developed to get the best beam pattern for changing soil moisture conditions.

Optimum UG Angle: The optimum angle to maximize UG2UG lateral wave communication is obtained as a function of the properties of soil medium by using (9). We analyze the lateral wave angle for silty clay loam and sandy soils for volumetric water content range of 0% to 40% in the frequency range of 100 to $1,000$ MHz. Particle distribution of these two soils is shown in the Table II.

Algorithm 1 SMABF Beam Steering Algorithm

Initialization :
Let A be the set of AG nodes
Let U be the set of the UG nodes
Let R be the receiver node
Sense the soil moisture level and determine the appropriate wavelength in soil
Select the array layout based on wavelength
Activate desired elements based on soil moisture and desired beam patterns
Produce the initial weights to achieve the desired beam pattern
Calculate the excitation and current distribution (root matching, pole-residue)
BEGIN
if R $\in$ A then **then**
  if θ_R is known **then**
    $AF(\theta,\phi) = \sum_{i=1}^{N} w_i exp(-\left[jk_s r_i(x_i\sin\theta\cos\phi + y_i\sin\theta\sin\phi)\right] + \delta_i)$
  else if
  then
    Normal to the surface beam using $AF(\theta,\phi) = \sum_{i=1}^{N} w_i exp(-\left[jk_s r_i(x_i\sin\theta\cos\phi + y_i\sin\theta\sin\phi)\right])$,
  end if
else if R $\in$ U **then**
  BEGIN
  Sense soil moisture
  Determine optimal angle using $\theta_{UG} = \frac{1}{2}\tan^{-1}\left(\frac{2Re(n^2-1)^{1/2}}{|n^2-1|-1}\right)$
  Output UG2UG Beam
  END
end if
Optimize to get low side lobe levels when wavelength changes
Optimize element positions
Activate virtual arrays
Adjust weights and excitation
Repeat this process to adjust these parameters when soil moisture changes
END

TABLE II: Particle Size Distribution and Classification of Testbed Soils.

Textural Class	%Sand	%Silt	%Clay
Sandy Soil	86	11	3
Silty Clay Loam	13	55	32

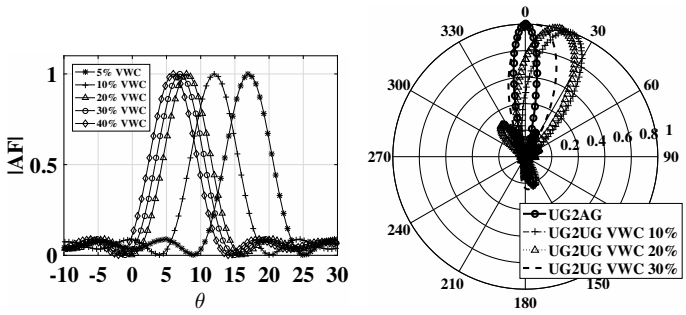

(a) (b)

Fig. 8: (a) Array factor for UG2UG communications for different soil moisture levels, (b) UG2AG Communications.

In Fig. 7, optimal angle for different soils are shown as function of frequency for soil moisture (VWC) range of 0 to 40%. It can be observed that optimal angle is high in the silty clay loam soil as compared to sandy soils. In silty clay loam soil it goes up to 16°, whereas in sandy soil it is 9°. This is explained by the higher dielectric constant of the silty clay soil as compared to the sandy soil. It can also be observed that optimal angle decreases with increase in soil moisture and it becomes close to zero when soil moisture (VWC) reaches to 40%. This is also attributed to increase in permittivity of soil due to increase in soil moisture. Summary of steering angles for UG2UG and UG2AG communications is given in Table I. UG beam patterns for different soil moisture levels are shown in Fig. 8(a)-8(b). In Fig. 8(a), linear plot of UG2UG array factor for different VWC values is shown. Polar plot with broadside UG2AG beam is shown in Fig.8(b). Next, enhancement in UG2UG communications are validated through empirical evaluations in silty clay loam and sandy soil.

Empirical Validation of Lateral Wave Enhancement Through Optimum UG Angle: To validate the lateral wave enhancement, experiments are conducted in the indoor testbed (Fig. 3) in the sandy soil and in the outdoor testbed in the silty clay soil(SCL). Particle distribution of these two soils is shown in the Table II. By using the directional antenna buried at the $20\,\mathrm{cm}$ depth. Measurements are conducted using the Keysights's Fieldfox Vector Network Analyzer (VNA) N9923A. Chanel transfer functions are recorded and channel gain is measured first with out the orientation change and then experiments are repeated by determining the optimum lateral wave angle in both soils. VWC values for sandy and silty clay loam soil 37% and 0%, respectively which gives the optimum angle of 4° in sandy soil and 16° in silty clay loam soil.

In Figs. 9, channel gain results of an experiment conducted in silty clay loam and sandy soils are shown for $50\,\mathrm{cm}$ and $1\,\mathrm{m}$ transmitter receiver (T-R) distance. It can be observed that energy is directed at 4° in sandy soil, a gain of $4\,\mathrm{dB}$ is realized at $500\,\mathrm{MHz}$ as compared to no orientation at $50\,\mathrm{cm}$ (Fig.9(a)). It can be observed that gain, by focusing energy in UG optimum angle, is higher at higher frequencies, because soil path of the wave are more effected by permittivity of soil. In Fig.9(b), channel gain in sandy soil for $1\,\mathrm{m}$ distance is shown. It can be observed that for at $1\,\mathrm{m}$, higher gain is achieved as compared to $50\,\mathrm{cm}$ because the lower contribution by the direct wave and communications is enhanced through optimum angle lateral wave.

Higher improvement in channel gains are observed in silty clay loam soil at $50\,\mathrm{cm}$ and $1\,\mathrm{m}$ distance (Fig.9(c)-Fig.9(d)) as compared to sandy soil. Silty clay loam soil has higher losses due to high permittivity of soil, therefore high channel gain is observed in UG lateral enhancement.

SMABF vs. Nonadaptive Beamforming: In this section, we compare performance of a SMABF 5×5 planar array with the beamforming system which does not adapt its parameters to soil moisture variations. Impact of soil moisture variations on array factor and directivity are investigated.

Element weights for a 5×5 planar array in soil for broadside UG2AG pattern, for 40% soil moisture level, at 433 MHz are shown in Fig. 10.

In Fig. 11 and Fig. 12, deterioration in array factor in sandy soil with change in soil moisture for a nonadaptive beamforming is shown in sandy and silty clay loam soil. The soil moisture VWC range is from 5% to 40%. In both soils, higher side lobes are observed when soil moisture increases from 5% to 40%. However, in sandy soil these effects of the change in soil moisture are less severe as compared to the silty clay soil. This is caused by larger wavelength changes due to soil moisture variations induced higher silty clay loam soil's permittivity.

In Fig. 13(a), directivity of SMABF is compared with nonadaptive beamforming system for different soil moisture levels in sandy and silty clay loam soils. It can be observed that the SMABF system is able to adapt to soil moisture changes to maintain its directivity whereas drastic changes are observed for nonadaptive system. In silty clay loam soil, when soil moisture increases higher than 5%, directivity remains less than the SMABF. However, in sandy soil for 10% and 30% soil moisture level, it becomes equal to the SMABF and even exceeds at 20%. This happens because SMABF in this comparison does not maximize the directivity, rather it just adapts to the wavelength changes caused by soil moisture variations by selecting corresponding inter-element spacing through forming virtual arrays. Directivity in SMABF can be maximized by optimization the inter-element spacing which maximize directivity for a given soil moisture level. SMABF virtual arrays and directivity optimization issues are discussed next.

SMABF Element Thinning Through Virtual Arrays: SMABF uses array thinning virtual arrays to adapt to soil moisture variations. In UG array thinning, an elements subset from full planar structure is selected to avoid grating lobes based on the optimization approach. Through element thinning, virtual arrays of elements are formed, where the physical antenna elements are turned on or off. By using this approach optimum configuration elements is determined to form the current soil moisture level. Element weights w_i are turned on

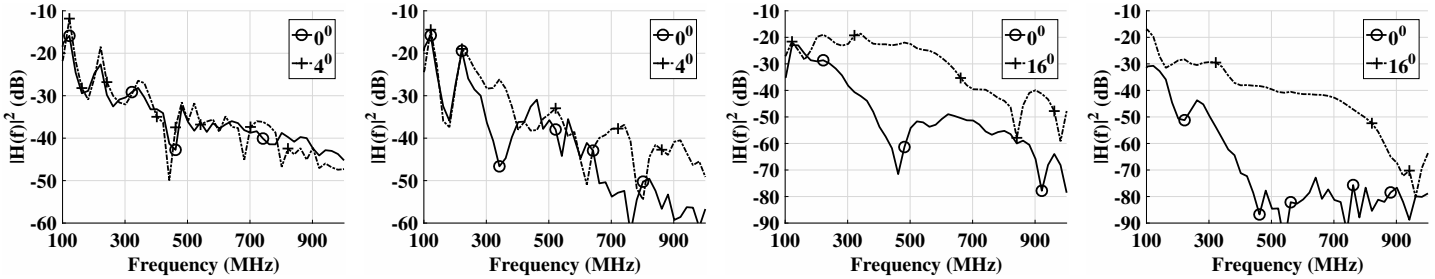

(a) Sandy - 50 cm T-R Distance (b) Sandy - 1 m T-R Distance (c) SCL - 50 cm T-R Distance (d) SCL - 1 m T-R Distance

Fig. 9: Comparison of optimum angle UG communications with fixed orientation.

and off as following:

$$w_i = \begin{cases} 1 & \text{if } d = \lambda_s/2, \\ 0 & otherwise. \end{cases} \tag{13}$$

where λ_s is the wave length in soil, and d is the distance of current (i^{th}) element to previous element and d is chosen such that with change in wavelength due to soil moisture variations, half-wave length inter-element spacing is maintained. At 433 MHz, variations in SMABF half wavelength inter-element spacing with 10% to 40% change in volumetric water content (VWC) are shown in Table III. Array operates with initial configurations and then adaptive thinning is done based on soil moisture changes. Virtual SMABF array helps to maintain side-lobe levels and fixed directivity. It also avoids high side-lobe distortions as observed in nonadaptive beamforming case.

SMABF Directivity Maximization: Fixed directivity limitation of virtual arrays can be improved by directivity maximization. With soil moisture change, the goal is to optimize the inter-element spacing which maximize directivity and avoids

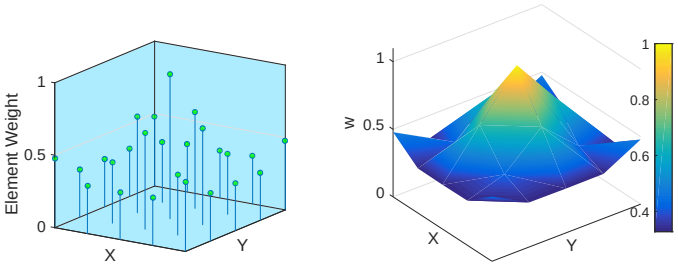

(a) (b)

Fig. 10: Element weights for a 5×5 planar array in soil for broadside UG2AG pattern, for 40% soil moisture level, at 433 MHz (a) Stem plot (b) Surf Plot.

TABLE III: Variations in SMABF half wavelength inter-element spacing with change in soil moisture. All values are in cm.

	Volumetric Water Content (VWC)			
Soil Type	**10%**	**20%**	**30%**	**40%**
Silt Loam	30.79	23.72	20.25	18.03
Sandy	46.83	39.28	34.62	31.28
Silty Clay Loam	27.86	20.53	17.12	15.01

(a) 5% (b) 10% (c) 20% (d) 30% (e) 40%

Fig. 11: Deterioration of array factor in SCL soil with change in soil moisture for a nonadaptive beamforming system.

(a) 5% (b) 10% (c) 20% (d) 30% (e) 40%

Fig. 12: Deterioration of array factor in sandy soil with change in soil moisture for a nonadaptive beamforming system.

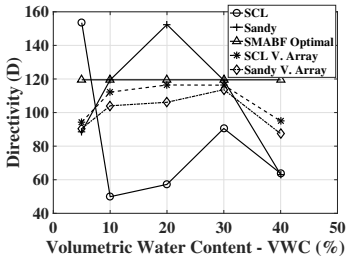

Fig. 13: Change in directivity in silty clay soil and sandy soil with change in soil moisture.

grating lobes. This optimization problem is formulated as:

$$\wp: \quad maxD = \frac{4\pi |AF_{max}|^2}{\int_0^{2\pi}\int_0^{\pi} |AF|^2 \sin\theta d\theta d\phi}, \tag{14}$$

$$s.t. \quad \frac{d}{\lambda_s} < \frac{1}{1+\sin\theta} \tag{15}$$

where D is directivity, θ is the steering angle for UG2UG and UG2AG communications from the broadside, d is inter-element spacing, λ_s is the wavelength in soil.

By using genetic algorithms [32], which work on the natural selection process. By using this technique, an initial inter-element position can either be specified or chosen arbitrarily. A priori position can be based on the actual position without consideration of the particular soil moisture level. Cost (score) function is evaluated and desired inter-element spacing is determined.

Feedback Control: In addition to soil moisture adaptive wights which are based on soil moisture sensing, feedback signals are used to adjust the weights by using the array gain feedback loops. This problem is formulated as maximize the

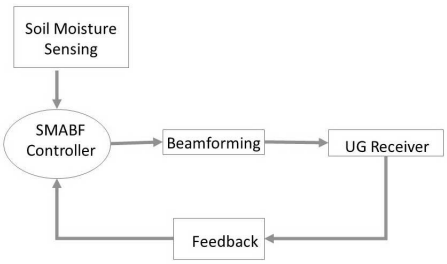

Fig. 14: SMABF with feedback.

array gain by using the pilot signals. In this method, SMABF array at the transmitter receives the pilot signal in receive mode and then accordingly adjusts its parameters for the transmit mode. In receive mode at the transmitter, scan angles are varied to to get the estimate of channel state. The best SNR statistics are used and with change in soil moisture, parameters are adjusted accordingly. In Fig. 14, SMABF control with feedback is shown. Received power at a UG receiver is given in Appendix D.

Adaptive SMABF Element Weighting: Signals of array elements of beamforming antennas can be controlled to produce the desired beam by phase and amplitude weighting [24]. In SMABF, current environment and the soil moisture information is used to weight the elements which leads to improvements in received SNR. Adaptive weight adjustment is done to keep the desired UG2UG and UG2AG characteristics based on the soil moisture variations.

Soil moisture adaptive weights are expressed as:

$$\boldsymbol{w} = \{w_0, w_1, w_2 ... w_{n-1}\}^T \tag{16}$$

Permittivity of the soil changes with the change in soil moisture and hence the wavelength. Weight factor γ_s is defined as:

$$\gamma_s = \frac{1}{\lambda_s} \times d \times \pi \times sin\theta_0 \tag{17}$$

where d is the inter-element distance. Accordingly, with this weight factor, i^{th} soil moisture adaptive weight w^i_{sm} becomes:

$$w^i_{sm} = \alpha_i exp(-j\gamma_s(2i - n - 1)) \tag{18}$$

where α_i is the element coefficient. These element coefficients are optimized to obtain desired sidelobe levels and beam patterns through element thinning and positioning approach. Once the beamforming vector is populated with the adaptive weights, then the desired beam pattern is produced as following:

$$F = \boldsymbol{X} w^i_{sm} \tag{19}$$

where $\boldsymbol{X}$ is the intended signal. To repeat this process with soil moisture change, gradient method is used. In this method, soil moisture adaptive weights are adjusted for next $(l + 1)$ iteration as following [24]:

$$w^i_{sm,l+1} = w^i_{sm,l} + s(-\nabla_l) \tag{20}$$

where s ensures stability and convergence and ∇_l is the gradient estimate vector. It is well known that performance of an adaptive antenna array system degrades with faster adaption [24]. Since soil moisture is a slowly varying process, this simple-to-implement approach exhibits minimum noise and high tolerance to performance degradation caused by faster adoption due to limited sampling.

SMABF Element Excitation: In addition to wavelength, and element position optimization, current excitation also needs to optimized for in SMABF. Due to the soil moisture variations, use of conventional excitation distributions (Uniform, Dolph/Chebyshev, Binomial, Taylor, Hansen, Tseng, Bayliss, separable, radial taper, radial taper squared) may lead to degraded beam patterns with soil moisture variations. Therefore, in this section we develop a soil moisture adaptive SMABF excitation method to get maintain the desired pattern. This method works as follows:

First, an initial current distribution w^0_i is found for the desired pattern by using the root matching method [40]. Once the soil moisture changes, the new patten is determined. Since soil moisture does not vary drastically with time and new pattern vary gradually from the old one with change in soil moisture in small angle steps, the w_i can be expressed as minor variations δw_i to the w^0_i:

$$w_i = w^0_i \ \pm \ \delta w_i \tag{21}$$

Since the current and desirable patterns are known, the pattern difference equation is solved using the matrix inversion method to obtain the δw_i, which is then used to get the new current which are used to give new pattern. This method can be repeated iteratively until the desired beam pattern is achieved. To further improve the pattern, a feedback method can be used, which is explained next.

In the next section, we present SMABF simulations.

IX. Simulations

In this section, SMABF design is investigated through simulations in CST Microwave Studio (MWS), a simulation program which is used to simulate full wave 3D EM problems.

A SMABF phased array antenna consisting of 5×5 dipole element has been simulated in sandy soil. Array is capable of operating on 0.2 - 0.6 GHz and supports the beam steering for the communication links and angles given in Table I to maintain connectivity with UG and AG nodes.

Since the properties of the array such as radiation pattern, operating bandwidth and S-parameters are determined from the proprieties of the individual element, therefore, we first simulated a dipole antenna in the sandy soil and different parameters are analyzed. Element is modeled using PEC cylinder material. Excitation is done using port placed in the gap in the middle of the element. Resonant frequency at one half-wavelength is 433 MHz. Higher mesh (40 per wavelength) is used for higher accuracy and time-domain solver is used using unit cell approach. 50-ohms feed impedance is used. S-parameters of the simulated element are compared with measurements to validate the simulated element design. Simulated and measured results (discussed in Section VI) shows a good agreement. Analysis of the simulated element verifies that with

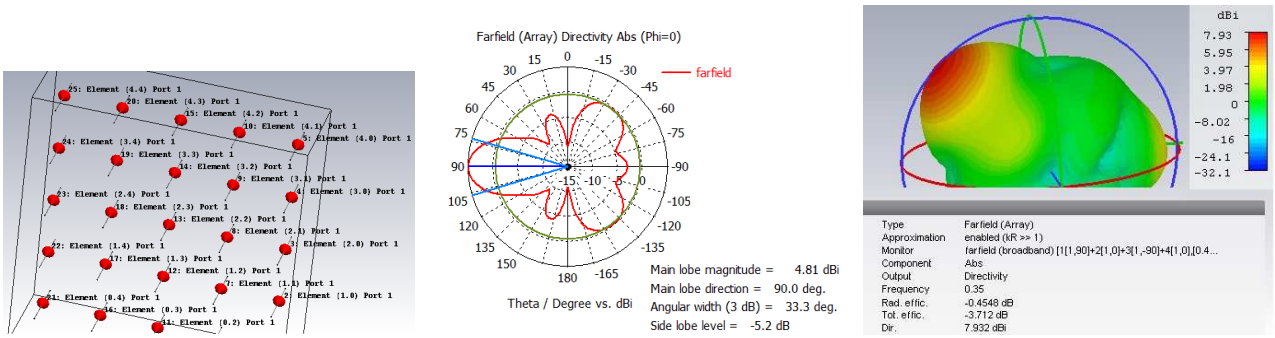

(a) (b) (c)

Fig. 15: (a) Design of 5×5 array in CST MWS, (b) UG2AG far-field simulated in CST MWS, (c) 3D view of UG2AG Beam,

the decrease in soil moisture, resonant frequency shifts to the lower end of the frequency spectrum and reflection coefficient and bandwidth also vary with change in soil moisture. Further details about these impacts can be found in Section VI).

Once the individual SMABF element is simulated and verified, then a full array simulation configuration is created to incorporate element into the array design. Simulated array is shown in Fig. 15(a). In CST MWS, once the UG2UG and UG2AG beam patterns are specified, then a distribution matrix can be calculated. This distribution matrix is used for element excitation to generate the desired beam pattern. With change in soil moisture, a new distribution matrix is produced to to adjust the beam steering angle and this process is repeated for dynamic adaption of soil moisture variation.

In Fig. 15(b), simulation results for UG2AG far-field are shown with beam parameters and 3D view is shown in Fig. 15(c). It can be observed that simulation results verify the beam synthesis analysis of Section. VII. Experimental results are reported in the next section.

X. SMABF Implementation

In this section, we discuss software and hardware implementation aspects of the SMABF.

Software Defined Implementation: Recent advancements in SDR technology and digital equipment allows efficient implementation of SMABF. Through software defined control of individual array elements, steering solutions can be used for communications with static and mobile AG devices. Moreover, complex algorithm processing capabilities can be implemented easily. SDR implementation [20] of UG beamforming is challenging due to many reasons. The major challenge is the phase shift between antenna elements. To get a desired beam pattern, the phase shifts between antenna elements needs to be equal in the desired direction. This requires calibration of phase shifters and dynamic on-the-fly synchronization and phase correction to achieve the desired beam.

Digital beamforming based on soil moisture conditions to form dynamic beam patterns can be used. This design consists of a planar array with its own phase shifter with pre-defined parameters for communication with UG and AG arrays. Furthermore beams can be stitched such that a number of beam patterns can be determined and designed based on the analyses of UG and AG devices and can be stored in configuration database for on-demand usage.

Another SDR approach is based on phase shifting done in the software. This approach is based on processing in the software defined radio to adapt to wavelength changes due to soil moisture conditions. The advantage of using this approach is that dynamic changes in the wavelength and phase variations due to UG channel dynamism are compensated without changing physical array arrangements. Moreover, less energy be required in comparison to traditional mechanical phase shifters [30].

Hardware Components: For SMABF hardware array elements can use dipole and printed circuit antennas. Other microwave components such as phase shifters, amplifiers, dividers, and hybrids can also be implemented as printed circuits through inexpensive equipment [30]. Beamforming network can consist of stripline configuration. Good wideband characteristics can be achieved within limited underground volume by using large diameter, closely spaced, conducting tubular SMABF elements. EM simulations, described in Section IX, can be used for design of prototype system. Use of resistive (dummy) elements at the edges of the array can be used to avoid performance degradation at the edge of the array due to abrupt changes. Once the simulated design meets the desired specifications, then an initial array layout configuration can be selected and optimized by observing the performance using a vector network analyzer. A vector network analyzer is used to measure the return loss (antenna reflection coefficients).

Obviously, any implementation of SMABF is a complicated and expensive as compared to existing solutions. Moreover, practical implementation of SMABF integrated with soil moisture sensing, and optimization is a challenging task. Decreasing cost and complexity of hardware, and importance of long range, high data rate UG communications, compared to conventional solutions, makes SMABF a viable candidate for next generation wireless UG communication systems.

XI. Conclusions

In this paper, soil moisture adaptive UG beamforming technique has been developed. UG channel model is analyzed

from UG beamforming perspective. It has been shown that lateral wave in UG communication when exploited using beamforming results in improved performance of the UG communications. Soil moisture variations, change in wavelength and directivity have been identified as main challenges in UG beam forming communications. Array factor is determined for UG2AG and UG2UG communications. A method has been developed to find the optimal angle to focus energy in the desired direction based on soil moisture changes. Array structure and element positioning are discussed and optimization approaches for SMABF are proposed. Empirical evaluations are done to investigate the optimum UG angle.

This work leads to some interesting research directions in the area of SMABF. First, the effects of coupling of soil-air interface on the UG2AG communications requires further analysis. Adjustments should be made to the array factor to account for this refection phenomena. Second, SMABF combined with power control, extension of this analysis to the receiving arrays due to antenna reciprocity principal, mutual coupling between array elements, simultaneous transmit and receive functionality, and impedance matching present other interesting research directions.

XII. Acknowledgments

This work is partially supported by a NSF CAREER award (CNS-0953900), NSF CNS-1423379, NSF CNS-1619285, NSF CNS-1247941 and a NSF CyberSEES grant (DBI-1331895).

Appendix A
Derivation of Optimal Angle

The effective permittivity of soil-water mixture, which is a complex number, can be modeled as [41]:

$$\epsilon_s = \epsilon_s' - i\epsilon_s'' \ , \tag{22}$$

$$\epsilon_s' = \begin{cases} 1.15\Big[1+\rho_b/\rho_s\left(\epsilon_s^{\delta}-1\right)+(m_v)^{\nu'}(\epsilon_{fw}')^{\delta}- \\ \quad m_v\Big]^{1/\delta} - 0.68 \qquad 0.3\,\mathrm{GHz} \le f \le 1.4\,\mathrm{GHz} \\ \Big[1+\rho_b/\rho_s\left(\epsilon_s^{\delta}-1\right)+(m_v)^{\nu'}(\epsilon_{fw}')^{\delta}-m_v\Big]^{1/\delta} \\ \qquad\qquad 1.4\,\mathrm{GHz} \le f \le 18\,\mathrm{GHz} \ , \end{cases} \tag{23}$$

$$\epsilon_s'' = \Big[(m_v)^{\nu''}(\epsilon_{fw}'')^{\delta}\Big]^{1/\delta} \ , \tag{24}$$

where f is the frequency in Hz, ϵ_s is the relative complex dielectric constant of the soil-water mixture, m_v is the volumetric water content, ρ_b is the bulk density and ρ_s is the particle density, δ, ν' and ν'' are empirically determined soil-type dependent constants given by

$$\delta = 0.65 \ , \tag{25}$$

$$\nu' = 1.2748 - 0.519S - 0.152C \ , \tag{26}$$

$$\nu'' = 1.33797 - 0.603S - 0.166C \ , \tag{27}$$

where S and C represent the mass fractions of sand and clay, respectively. The quantities ϵ_{fw}' and ϵ_{fw}'' in (23) and (24) are the real and imaginary parts of the relative permittivity of free water, and are calculated from the Debye model [41]:

$$\epsilon_{fw}' = e_{w\infty} + \frac{\epsilon_{w0}-\epsilon_{w\infty}}{1+(2\pi f\tau_w)^2} \ , \tag{28}$$

$$\epsilon_{fw}'' = \frac{2\pi f\tau_w(\epsilon_{w0}-\epsilon_{w\infty})}{1+(2\pi f\tau_w)^2} + \frac{\delta_{eff}}{2\pi\epsilon_0 f}\frac{(\rho_s-\rho_b)}{\rho_s m_v} \ , \tag{29}$$

where $\epsilon_{w\infty} = 4.9$ is the limit of ϵ_{fw}' when $f \to \infty$, ϵ_{w0} is the static dielectric constant for water, τ_w is the relaxation time for water, and ϵ_0 is the permittivity of free space. Expressions for τ_w and ϵ_{w0} are given as a function of temperature. At room temperature (20°C), $2\pi\tau_w = 0.58\times10^{-10}$s and $\epsilon_{w0} = 80.1$. The effective conductivity, δ_{eff}, in (29) in terms of the textural properties of the soil, is given by

$$\delta_{eff} = \begin{cases} 0.0467 + 0.2204\rho_b - 0.4111S + 0.6614C \\ \qquad\qquad 0.3\,\mathrm{GHz} \le f \le 1.4\,\mathrm{GHz} \ . \\ -1.645 + 1.939\rho_b - 2.25622S + 1.594C \\ \qquad\qquad 1.4\,\mathrm{GHz} \le f \le 18\,\mathrm{GHz} \ , \end{cases} \tag{30}$$

This angle depends on these dielectric properties of the soil and is given as [39]:

$$\theta_{UG} = \frac{1}{2}\tan^{-1}\left(\frac{2Re(n^2-1)^{1/2}}{|n^2-1|-1}\right)rad, \tag{31}$$

where n is the refractive index of the soil and is given as

$$n = \sqrt{\frac{\sqrt{\epsilon'^2+\epsilon''^2}+\epsilon'}{2}} \ , \tag{32}$$

in which ϵ' and ϵ'' are the real and imaginary parts of the relative permittivity of the soil.

Appendix B
Wavenumber in Soil

Wavenumber in soil is given as:

$$k_s = \beta_s + i\alpha_s \tag{33}$$

where β_s indicates phase shift and α_s indicates propagation losses. Alternatively,

$$k_s = \omega\sqrt{\mu_0\epsilon_s} \tag{34}$$

where $\omega = 2\pi f$, and f is the frequency of the wave; μ_0 and ϵ_s are the permeability and permittivity of the soil, respectively.

Appendix C
Speed of Wave in Soil

Speed of the wave in soil is given as [1]:

$$S = c/n, \tag{35}$$

where

$$c = 3\times10^8 \ m/s \tag{36}$$

is the speed of light, n is the refractive index of soil given by (32) with ϵ' and ϵ'' are the real and imaginary parts of the relative permittivity of the soil.

APPENDIX D
DERIVATION OF POWER RECEIVED AT UG NODE

The SMABF effective isotropic radiated power (EIRP) can be expressed as product of the transmitted power and antenna gain:

$$P_{rad} = G_t P_t, \tag{37}$$

where P_t is the transmitted power and G_t is the array gain.

The far-field power density P_{av} can is expressed as [38]:

$$P_{av} = P_{av}^D + P_{av}^R + P_{av}^L \ . \tag{38}$$

where D, R, L denotes the power densities of the direct, reflected and lateral component [1]. The received power is calculated as the product of far-field power density P_{av} and antenna aperture ($\lambda_s^2/4\pi$). The received power is given as [38]:

$$\begin{aligned} P_r^d &= P_t + 20\log_{10}\lambda_s - 20\log_{10} r_1 - 8.69\alpha_s r_1 \\ &\quad -22 + 10\log_{10} D_{rl} \ , \\ P_r^r &= P_t + 20\log_{10}\lambda_s - 20\log_{10} r_2 - 8.69\alpha_s r_2 \\ &\quad +20\log_{10}\Gamma - 22 + 10\log_{10} D_{rl} \ , \\ P_r^L &= P_t + 20\log_{10}\lambda_s - 40\log_{10} d - 8.69\alpha_s(h_t + h_r) \\ &\quad +20\log_{10} T - 22 + 10\log_{10} D_{rl} \ , \end{aligned} \tag{39}$$

where Γ and T are reflection and transmission coefficients [38], and λ_s is the wavelength in soil. The received power, for an isotropic antenna, is expressed as [38]:

$$P_r = 10\log_{10}(10^{\frac{P_r^d}{10}} + 10^{\frac{P_r^r}{10}} + 10^{\frac{P_r^L}{10}}) \ . \tag{40}$$

For an array of identical elements, the far-field power density is expressed as [30]:

$$P_{den} = \frac{|E(\theta,\phi)|^2}{120\pi}, \tag{41}$$

where $E(\theta,\phi)$ is the electric filed intensity of the individual array element and is given as:

$$|E(\theta,\phi)| = \sqrt{P_{et}}\sqrt{G_{et}}\frac{\sqrt{30}}{d}, \tag{42}$$

where P_{et}, G_{et} are element transmit power and gain, respectively, and d is the distance. E-field contributions (E_a) from all elements are added together to calculate the array gain G_a [30]. Therefore,

$$G_a(\theta,\phi) = \frac{d^2}{30}\frac{|E_a \ \varsigma(\theta,\phi)|^2}{P_t}, \tag{43}$$

where ς is the element phase factor and

$$E_a = \frac{\sqrt{30}}{d}\sum_n \sqrt{P_{et}}\sqrt{G_{et}}. \tag{44}$$

REFERENCES

[1] A. Salam, M. C. Vuran, and S. Irmak, "Pulses in the sand: Impulse response analysis of wireless underground channel," in *Proc. INFOCOM 2016*, San Francisco, USA, Apr. 2016.

[2] X. Dong and M. C. Vuran, "Impacts of soil moisture on cognitive radio underground networks," in *Proc. IEEE BlackSeaCom*, Georgia, 2013.

[3] F. Tokan and et.al., "The lateral wave antenna," *IEEE Transactions on Antennas and Propagation*, vol. 62, no. 6, pp. 2909–2916, June 2014.

[4] M. J. Tiusanen, "Wideband antenna for underground Soil Scout transmission," *IEEE Antennas and Wireless Propagation Letters*, vol. 5, no. 1, pp. 517–519, December 2006.

[5] I. F. Akyildiz and E. P. Stuntebeck, "Wireless underground sensor networks: Research challenges," *Ad Hoc Networks Journal*, July 2006.

[6] I. F. Akyildiz, Z. Sun, and M. C. Vuran, "Signal propagation techniques for wireless underground communication networks," *Physical Communication Journal (Elsevier)*, vol. 2, no. 3, pp. 167–183, Sept. 2009.

[7] Z. Sun and I. Akyildiz, "Magnetic induction communications for wireless underground sensor networks," *Antennas and Propagation, IEEE Transactions on*, vol. 58, no. 7, pp. 2426–2435, July 2010.

[8] X. Dong, M. C. Vuran, and S. Irmak, "Autonomous precision agricultrue through integration of wireless underground sensor networks with center pivot irrigation systems," *Ad Hoc Networks (Elsevier)*, 2012.

[9] H. R. Bogena, M. Herbst, J. A. Huisman, U. Rosenbaum, A. Weuthen, and H. Vereecken, "Potential of wireless sensor networks for measuring soil water content variability," *Vadose Zone Journal*, Nov. 2010.

[10] H. Guo and Z. Sun, "Channel and energy modeling for self-contained wireless sensor networks in oil reservoirs," *IEEE Trans. Wireless Communications*, vol. 13, no. 4, pp. 2258–2269, April 2014.

[11] A. Markham and N. Trigoni, "Magneto-inductive networked rescue system (miners): Taking sensor networks underground," in *Proceedings of the 11th ICPS*, ser. IPSN '12. ACM, 2012, pp. 317–328.

[12] Z. Sun and I. Akyildiz, "Channel modeling and analysis for wireless networks in underground mines and road tunnels," *IEEE Trans. on Communications*, June 2010.

[13] Z. Sun, P. Wang, M. C. Vuran, M. A. Al-Rodhaan, A. M. Al-Dhelaan, and I. F. Akyildiz, "Border patrol through advanced wireless sensor networks," *Ad Hoc Networks*, vol. 9, no. 3, pp. 468–477, 2011.

[14] Z. Sun and et.al., "MISE-PIPE: Magnetic induction-based wireless sensor networks for underground pipeline monitoring," *Ad Hoc Networks*, 2011.

[15] M. C. Vuran and I. F. Akyildiz, "Channel model and analysis for wireless underground sensor networks in soil medium," *Physical Communication*, vol. 3, no. 4, pp. 245–254, December 2010.

[16] X. Tan, Z. Sun, and I. F. Akyildiz, "Wireless underground sensor networks: Mi-based communication systems for underground applications." *IEEE Antennas and Propagation Magazine*, vol. 57, no. 4, Aug 2015.

[17] X. Liu and et.al., "DIRC: increasing indoor wireless capacity using directional antennas," *SIGCOMM Comput. Commun. Rev.*, Aug. 2009.

[18] S. Lakshmanan, K. Sundaresan, R. Kokku, A. Khojestepour, and S. Rangarajan, "Towards adaptive beamforming in indoor wireless networks: An experimental approach," in *INFOCOM 2009, IEEE*, April 2009.

[19] D. Kontaxis and et.al., "Optimality of transmit beamforming in spatially correlated mimo rician fading channels," *Wir. Per. Comm.*, 2016.

[20] F. Quitin and et.al., "A scalable architecture for distributed transmit beamforming with commodity radios: Design and proof of concept," *IEEE Trans. on Wireless Communications*, March 2013.

[21] T. Nitsche and et.al., "Steering with eyes closed: Mm-wave beam steering without in-band measurement," in *IEEE INFOCOM*, April 2015.

[22] N. Anand, S.-J. Lee, and E. W. Knightly, "Strobe: Actively securing wireless communications using zero-forcing beamforming," in *INFOCOM, 2012 Proceedings IEEE*, March 2012, pp. 720–728.

[23] E. Aryafar and et.al., "Adam: An adaptive beamforming system for multicasting in wireless lans," *IEEE/ACM Trans. on Networking*, 2013.

[24] B. Widrow and et.al., "Adaptive antenna systems," *Proceedings of the IEEE*, Dec 1967.

[25] G. C. Alexandropoulos, P. Ferrand, J. m. Gorce, and C. B. Papadias, "Advanced coordinated beamforming for the downlink of future lte cellular networks," *IEEE Communications Magazine*, July 2016.

[26] Y. Du and et.al., "iBeam: Intelligent client-side multi-user beamforming in wireless networks," in *IEEE INFOCOM 2014*, April 2014.

[27] S. Kisseleff, I. F. Akyildiz, and W. Gerstacker, "Beamforming for magnetic induction based wireless power transfer systems with multiple receivers," in *2015 IEEE GLOBECOM*, Dec 2015.

[28] R. W. P. King and G. Smith, *Antennas in Matter*. MIT Press, 1981.
[29] R. Hansen, *Phased Array Antennas*. Wiley, 2009.
[30] A. Fenn and P. Hurst, *Ultrawideband Phased Array Antenna Technology for Sensing and Communications Systems*. MIT Press, 2015.
[31] F. Gross, *Smart Antennas with MATLAB*. McGraw-Hill, 2015.
[32] R. Haupt, *Timed Arrays*. Wiley, 2015.
[33] M. Dobson and et.al., "Microwave dielectric behavior of wet soil—Part II: Dielectric mixing models," *IEEE Trans. Geoscience and Remote Sensing*, vol. GE-23, no. 1, pp. 35 –46, January 1985.
[34] M. C. Vuran, X. Dong, and D. Anthony, "Antenna for wireless underground communication," Jun. 25 2015, uS Patent App. 14/415,455. [Online]. Available: http://www.google.com/patents/US20150181315
[35] R. Mailloux, *Phased Array Antenna Handbook*. Artech House, 2005.
[36] L. C. Godara, "Application of antenna arrays to mobile communications. ii. beam-forming and direction-of-arrival considerations," *Proceedings of the IEEE*, vol. 85, no. 8, pp. 1195–1245, Aug 1997.
[37] R. W. P. King, M. Owens, and T. T. Wu, *Lateral Electromagnetic Waves*. Springer-Verlag, May 1992.
[38] X. Dong and M. C. Vuran, "A channel model for wireless underground sensor networks using lateral waves," in *Proc. of IEEE Globecom '11*, Houston, TX, December 2011.
[39] D. Staiman and T. Tamir, "Nature and optimisation of the ground (lateral) wave excited by submerged antennas," *Electrical Engineers, Proceedings of the Institution of*, vol. 113, no. 8, August 1966.
[40] R. S. Elliott, *Antenna Theory and Design*. Prentice-Hall, Inc., 1981.
[41] N. Peplinski, F. Ulaby, and M. Dobson, "Dielectric properties of soil in the 0.3–1.3 ghz range," *IEEE Transactions on Geoscience and Remote Sensing*, vol. 33, no. 3, pp. 803–807, May 1995.